

FORECASTING INFRAGRAVITY WAVE ENERGY WITHIN A HARBOUR

McComb, P.¹, Gorman, R.² and Goring, D.³

Abstract: The relationship between wave energy outside a harbour and the infragravity wave heights at the berths in a mooring basin was examined during a four-month wave measurement program at Port Taranaki, New Zealand. The field data indicate that the near infragravity energy band (IG <120 s) is linked to the wave breaking process, and is strongly modulated by the tide level. An empirical formula to predict the infragravity waves at the berths was developed, based on the offshore partial significant swell height, associated peak period, and the tidal water level ($R^2 \sim 0.8$). A regional wave model was used to forecast the swell height and period, and in turn predict the infragravity wave heights at the harbour berths. The prediction system provides a very clear and reliable indication of the timing and magnitude of upcoming infragravity events, has been implemented as an operational tool for Port Taranaki harbour management. The system could be applied to many of the harbour basins in the world that are affected by infragravity waves, subject to onsite calibration.

INTRODUCTION

Infragravity (or long) waves are often observed within harbours, particularly those located on coasts with energetic wave conditions. These low frequency waves have periods of greater than 25 seconds, and depending on the harbour configuration, can result in oscillations (seiches) which cause unacceptable vessel movements resulting in the breaking of mooring lines, fenders and piles, as well as ship damage (e.g. Wilson, 1972; Wiegell, 1964; Sawaragi and Kubo, 1982; Mei and Agnon, 1989; Wu and Liu, 1990; Morison and Imberger, 1992; Rabinovich, 1993).

Port Taranaki in New Zealand (Fig. 1), is sited within a high energy wave climate, on a coast that is exposed to long period swells from the Southern Ocean (McComb *et al.*, 1999). The presence of infragravity (IG) waves within the harbour is common, although the magnitude of this energy is usually low and not problematic to the port operations. However, occasionally the infragravity energy causes excessive motion in the moored ships, and these events typically occur over the high tide and within 24 hours of a storm

1 ASR Ltd, New Plymouth, New Zealand; p.mccomb@asrltd.co.nz

2 National Institute of Water and Atmospheric Research, New Zealand; r.gorman@niwa.co.nz

3 Mulgor Consulting Ltd, Christchurch, New Zealand; d.goring@mulgor.co.nz

peak. These occurrences necessitate the use of a specific shore-based mooring line configuration, rather than using the ships' own mooring lines.

In order to better manage the mooring of ships in this climate, and to optimise a Dynamic Under Keel Clearance system (DUKC), a program of study and field measurement was initiated in 2003. The aim of the work was to examine the causal relationship between wave activity outside the Port and the infragravity response of the mooring basin within the harbour. This knowledge would then allow a method of forecasting the problematic infragravity events to be developed.



Figure 1. Port Taranaki, New Zealand

BACKGROUND

There are three major mechanisms to transfer the energy of atmospheric processes into IG waves (Rabinovich, 1993): i) direct generation of long waves by atmospheric pressure or wind acting upon the sea surface; ii) transfer of low-frequency energy (e.g. storm surges) into higher frequencies by topographic and meteorological effects, and iii) transfer of swell energy to large-scale and lower-frequency motions due to non-linear frequency dispersion. IG waves generated by the last process are of interest in the present study.

It is widely accepted that IG waves are generated through the non-linear interaction of wind waves, either offshore of the surf-zone and/or in the surf zone through varying of the breaker location and concomitant setup. The resultant low frequency wave form is also referred to as 'surfbeat' by many authors. Numerous studies of IG waves have been made using analytical expressions and empirical formulations obtained from field measurements. The initial work by Munk (1949) and Tucker (1950) found a relationship between low frequency water level oscillations (i.e. 1-5 minute period) and the maximum wave height. Funke and Mansard (1979), Kimura (1980) and Goda (1983) have used an empirical approach to consider the effect of wave groupings on IG waves, while others have investigated the IG relationship to gravity wave characteristics, such as Vis (1985), Nelson *et al.* (1988), Medina (1990), Bowers (1982) and Lara *et al.* (2004). The empirical formulation for the long wave energy based on the gravity band energy is defined as:

$$H_{sIG} = \frac{H_s^a T_p^b}{h^x} \quad (1)$$

where H_{sIG} is the significant wave height for the IG band, H_s is the significant wave height for the gravity band, T_p is the peak period for the gravity band, h is the water depth and a , b and x are parameters.

IG waves can be further classified as: a) free waves (which are not locally-forced and are freely propagating) of which there are two types (i) edge-waves, that are reflectively

trapped to the shoreline, and (ii) leaky-waves, that escape out to deeper water upon reflection from the shoreline, and b) forced (or bound) waves, which are second-order forced waves generated by wave groups.

Free IG waves

The motion of the breakpoint results in large time-varying radiation stress gradients in the region of incipient breaking, which acts as a local forcing of free long waves at the group frequency and its higher harmonics. These free waves will propagate in the onshore and offshore directions in a process termed dynamic setup.

Edge and leaky waves have long wavelengths relative to their amplitudes, allowing for near-perfect reflection from the shoreline without breaking. These waves set up a standing wave structure with nodes and anti-nodes in the cross-shore and can be either progressive or standing in the longshore. The wave form of the different nodes becomes similar towards shore, and the waves have their largest amplitudes near the shoreline and decay exponentially offshore.

Leaky waves, like edge waves, are standing in the cross-shore direction but do not attenuate with distance offshore, thus they can theoretically have an infinite number of nodes and antinodes. These waves have a cross-shore structure similar in appearance to edge waves, particularly close to shore. High node edge waves have many nodes and antinodes and can be indistinguishable from leaky waves in the surf zone.

Bound IG waves (or FIG waves)

Bound IG waves (or far infragravity waves) are the water level set-down under groups of incident waves, having troughs that are beneath the larger waves of the group and crests in-between the wave groups (Longuet-Higgins and Stewart, 1962). They have the same periodicity as the wave group and travel at group velocity. While the FIG wave form is intrinsically linked (or bound) to the propagating swells, the variation in water level associated with the groupiness can cause seiching within a port or harbour as the wave groups propagate past an open entrance. These wave forms typically have lower frequencies than the IG surfbeat (i.e. periods 2-20 minutes) and are not considered in detail in the present study.

IG waves within harbours

An open-mouthed harbour has a fundamental mode of oscillation; the ‘zeroth’ mode as well as the ‘natural’ resonant periods (so called ‘eigen periods’) which are determined by the harbour bathymetry and shape. The eigen periods of a regular open mouth basin of length L and a uniform depth, h , are described by:

$$T_n = \frac{4L}{(2n+1)\sqrt{gh}}, \text{ for mode } n = 1, 2, 3 \dots \quad (2)$$

where g is the gravitational acceleration. For narrow-mouthed bays and harbours most energy with the long-wave spectrum tends to be concentrated within the zeroth mode. In the case of irregularly-shaped harbours with varying bathymetry (such as Port Taranaki), the simple definition of the resonant modes is not always possible. Indeed, individual regions within the harbour will have specific resonance periods, such as the harbour basin where ships are moored for example. Resonance within these regions is likely to be closer to that of a closed rectangular basin:

$$T_n = \frac{2L}{n\sqrt{gh}}, \text{ for mode } n = 1, 2, 3 \dots \quad (3)$$

Tidal modulation of IG waves

Several authors have observed an infragravity modulation over the tidal cycle. Most specifically, Okihiro and Guza (1995) found that IG energy levels were considerably higher at high tide. They speculate that the reason for the increase was the changing reflectivity of an adjacent beach (with a concave profile). The IG waves in the highest frequency band studied (i.e. 0.5-1.7 min) were 5-10 times more energetic at high tide than at low tide levels, both inside and outside of the harbours that were studied (tidal range ~2.5 m). Resonant frequencies in the harbour were also modulated, presumably due to the changing in water depth. Correlations between the offshore swell energy and the harbour IG levels were considerably improved when the stage of the tide was considered.

EXPERIMENTAL METHODS

Data collection

The data collection phase of the study ran from July – November 2003, and the location of the instrumentation is shown on Figure 2. An offshore wave boundary condition was measured with a Triaxys directional waverider (WR), moored some 23 km northeast of the Port in 50 m water depth. Spectra were obtained from 20-minute recording bursts at hourly intervals. Close to the harbour entrance in 8 m water depth, a wave recording platform (WT) recorded 2 Hz pressure data in 20-minute bursts each hour. On the ends of each of the harbour berths (B, NK, M), pressure sensors were positioned 1.5 m below the lowest tide level, and 2 Hz data logged over 20-minute bursts each hour. A tide gauge near the NK site recorded the 1-minute mean water level.

Forecasts of the directional wave spectra at the waverider site (WR) were provided using the New Zealand Regional WAM model (Gorman, 2005). This is a 3rd generation model, which accommodates the processes of wave generation by wind, energy dissipation by white-capping and seabed friction, and direct estimates of non-linear energy transfers through wave-wave interactions. The model is driven by the NCEP winds and the numerical domain is shown in Figure 3.

Data analysis

Infragravity wave statistics were derived from 20-minute data bursts (at 2 Hz), while the far infragravity values were derived from 60 minute bursts of 1-minute means. After atmospheric pressure correction, the burst time-series of pressures were converted to sea surface elevations by applying linear wave theory. This conversion involves filtering to correct for the depth of the instrument below the surface and filtering to remove frequencies above a depth-dependent cut-off,

$$f_{cut} = 0.282\sqrt{g/d} \quad (4)$$

where f_{cut} is the frequency cut-off, g is gravitational acceleration and d is the instrument depth below the surface. After detrending to remove the tidal signal, zero-down-crossing (zdc) analysis was applied to each measurement burst to establish a sequence of individual wave heights and periods. From these H_{z3} (mean of the largest 1/3 of wave heights) and T_{z3} (mean period of these waves) were computed. The zdc method was used for the IG and FIG waves in preference to a spectral technique because of the limited number waves per measurement burst.

Using the directional wave spectrum $S(f, \theta)$ measured at site WR, the 1-dimensional spectrum was obtained by integrating over directions:

$$S(f) = \int_0^{2\pi} S(f, \theta) d\theta \quad (5)$$

From the computed spectral energy density $S(f)$, the peak frequency f_p and peak energy $S_p = S(f_p)$ of the spectrum were located. Spectral moments

$$M_j = \int_0^{\infty} f^j S(f) df \quad (6)$$

were computed, allowing the following statistics to be defined:

$$\text{significant height} \quad H_s = 4\sqrt{M_0} \quad (7)$$

$$\text{mean period} \quad T_{m1} = M_0 / M_1 \quad (8)$$

$$\text{mean apparent period} \quad T_{m2} = \sqrt{M_0 / M_2} \quad (9)$$

$$\text{mean frequency} \quad f_{mean} = M_1 / M_0 \quad (10)$$

$$\text{mean crest period} \quad T_{cr} = \sqrt{M_2 / M_4} \quad (11)$$

$$\text{spectral width} \quad SW = 1 - \frac{M_2^2}{M_0 M_4} \quad (12)$$

Wavelet analysis was also applied to the 1-minute mean water levels measured by the tide gauge near site NK (see Goring, 2005 for analysis details). This method results in a contour map showing how the significant FIG wave height are distributed with time and period.

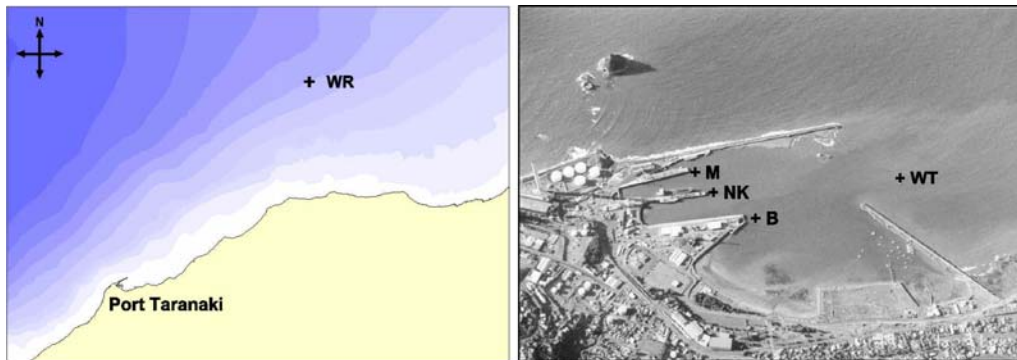


Figure 2. Location of wave recorders. WR is a waverider buoy moored 23 km from the Port in 50 m water depth. Pressure sensors were deployed near the entrance (WT) and on the ends of each berth (M, NK and B).

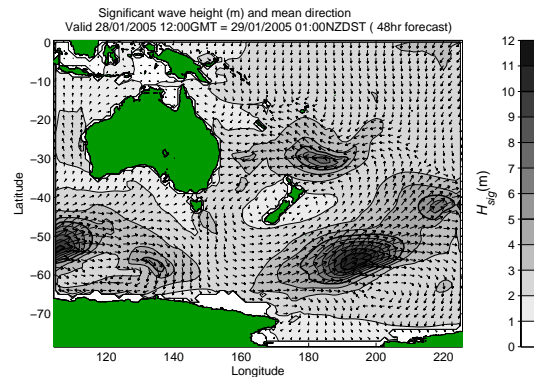


Figure 3. Example forecast of significant wave height and mean wave direction over the WAM numerical domain.

RESULTS

General observations

Analyses of the harbour wave data indicate that long waves are present in a continuum throughout the infragravity spectrum, exhibiting significant peaks within the near infragravity (IG <120 s) and far infragravity (FIG >120 s) bands. Wave energy in these two bands are associated with the incident swell, but they exhibit very different characteristics.

The data from site WT shows that IG waves near the harbour entrance typically have periods in the 30-90 s range, with a median zdc wave period (T_{z3}) of 51 s. The largest wave events have periods of 40-70 s, and the maximum zero-down-crossing wave heights (IG H_{z3}) was 0.47 m. A time-series of the IG H_{z3} measured within the harbour is shown on Figure 4, along with the significant wave heights (H_s) measured offshore by the waverider buoy and the heights measured at WT. The harbour IG waves clearly follow the deepwater wave height trends, but are strongly modulated by the tide level. The berth IG wave heights are all of a similar magnitude (although NK is the lowest) and are approximately half the height of the IG waves measured just outside the harbour entrance.

The water level variations due to very long period FIG waves (i.e. >120 s period) were observed to exceed 0.5 m in height (FIG H_{z3}) on occasion (Fig. 4), but do not exhibit a height modulation by the tide level, as do the IG waves. The FIG wave periods vary from 3-20 minutes, with predominance for the 11-15 minute band. Wavelet analysis over a three-hour window was used check the zdc method, and a large FIG event is depicted by the wavelet transformation in Figure 5. Water level variations at this frequency are not likely to cause mooring problems, but do represent a reduction to the available depth in the underkeel clearance.

Relating harbour infragravity wave heights to the offshore wave spectra

The measured IG waves within the harbour basin (i.e. sites B, NK and M) were compared with the directional spectral parameters recorded by the offshore waverider buoy. As expected, energetic swell conditions lead to energetic infragravity conditions within the harbour. However, these data have a poor statistical correlation and often exhibit a lag between the energy peaks (e.g. Fig. 4), further influenced by the tidal modulation of the IG wave heights. The tides at Port Taranaki are semi-diurnal with spring-neap range of 3.1 m.

To isolate the effect of tide level, a low-pass filter was applied and the residual time series of IG wave heights compared against various forms of Eqn. 1 including other spectral parameters (Eqns. 7-12). Ultimately, it was found that the best predictor of the residual IG wave heights was given by:

$$H_{sIG(res)} = m[H_{s(swell)}^{1.1} T_{p(swell)}^{0.5}] + c \quad (13)$$

where the H_s (swell) is the partial significant wave height (offshore deepwater) for frequencies <0.143 Hz, T_p (swell) is the associated peak period and m and c are the gradient and intercept. Notably, the deepwater wave direction was not important, although this may be due to the narrow directional range of the swell frequencies. The measured and predicted (non-tidal) time-series are presented in Figure 6 for site M, and the R^2 linear regression coefficients for each harbour basin site (M, NK and B) were all similar at 0.84-0.85. The tidal modulation of the IG waves was quantified by correlating the tide level against the IG wave height ratio of the non-tidal residual and total data. The modulating effect was found to be approximately linear, but with only ~60% of the variance explained. When combined with Eqn. 13, the predictor for IG wave heights within the harbour basin is:

$$H_{sIG} = H_{sIG(res)}yh \tag{14}$$

where the y is the modulating coefficient and h is the tide level relative to msl. Linear regression of the combined prediction system (Eqns. 13 and 14) for sites M, NK and B returns an R^2 correlation of 0.73, 0.77 and 0.80, respectively. The M site data are shown in time-series on Figure 6, and the coefficients in Eqns. 13 and 14 for all the basin sites are listed in Table 1.

Table 1. IG wave height prediction coefficients for the harbour

Site	Eqn. (13), m	Eqn. (13), c	Eqn. (14), y
M	0.0061	0.0174	0.2255
NK	0.0048	0.0188	0.1490
B	0.0065	0.0156	0.1768

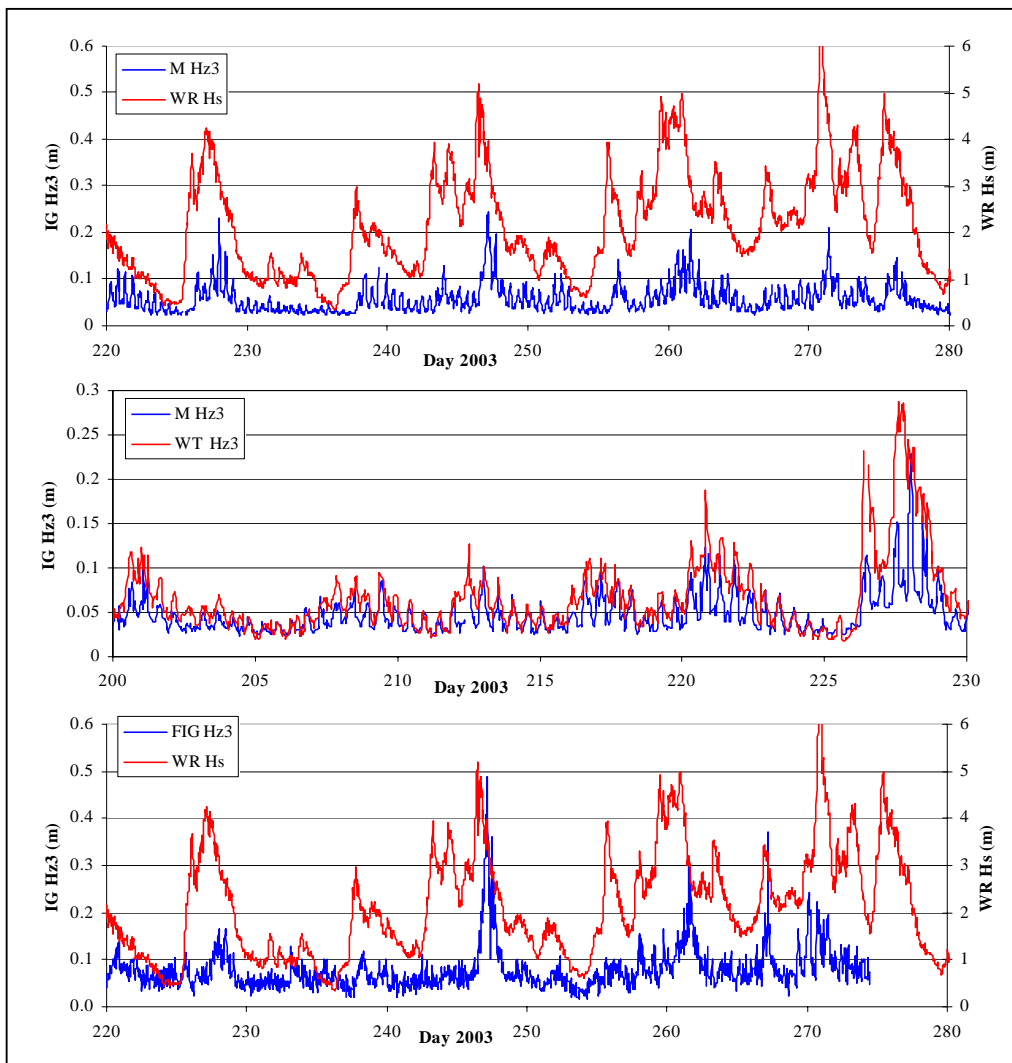


Figure 4. Time-series of the infragravity wave heights inside the harbour (site M) and the offshore (site WR) significant wave heights (top plot), plus the infragravity wave heights near the harbour entrance (site WT; lower plot).

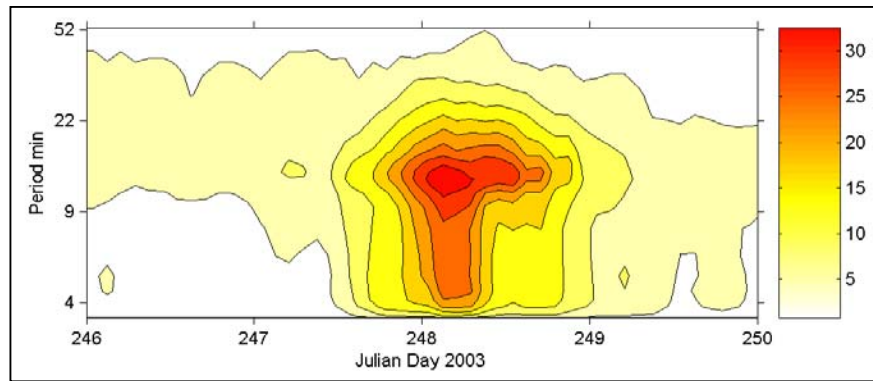


Figure 5. Wavelet analysis of the 1-minute tide gauge data, showing a 4 day period in which the largest FIG waves were measured. Contours are H_s (mm).

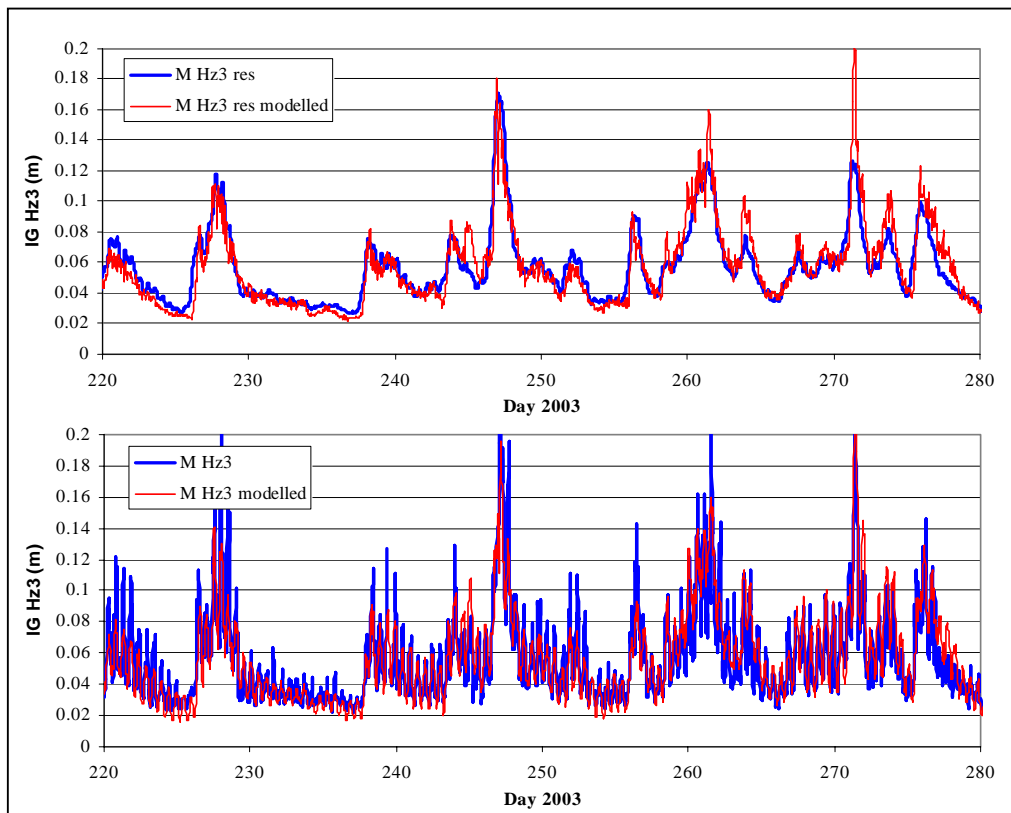


Figure 6. Time-series of the measured and modelled IG wave heights inside the harbour basin (site M). Upper plot shows the residual (non-tidal) data.

Forecasting infragravity waves

The forecast wave spectra were processed to extract the swell H_s and associated T_p and these values compared with those measured by the waverider buoy. In general, the WAM model was able to confidently predict the swell events up to 96 hours ahead, and reproduce $\sim 74\%$ of the total variance at 48 hours forecast. When coupled to Eqns. 13 and 14 to forecast the IG waves in the harbour, the system was found to predict all the major IG events up to 96 hours ahead. A forecast accuracy matrix was developed for increments up to 96 hours ahead, and the R^2 linear regression coefficients are listed in Table 2. A time-series of the measured and predicted IG waves (site M) is presented in Figure 7 for the 48 hour forecast condition.

Table 2. R^2 linear regression coefficients for the forecast IG waves heights in the harbour basin

Site	Nowcast	24 hr	48 hr	72 hr	96 hr
M	0.77	0.75	0.81	0.73	0.71
NK	0.73	0.72	0.76	0.69	0.64
B	0.75	0.75	0.82	0.71	0.70

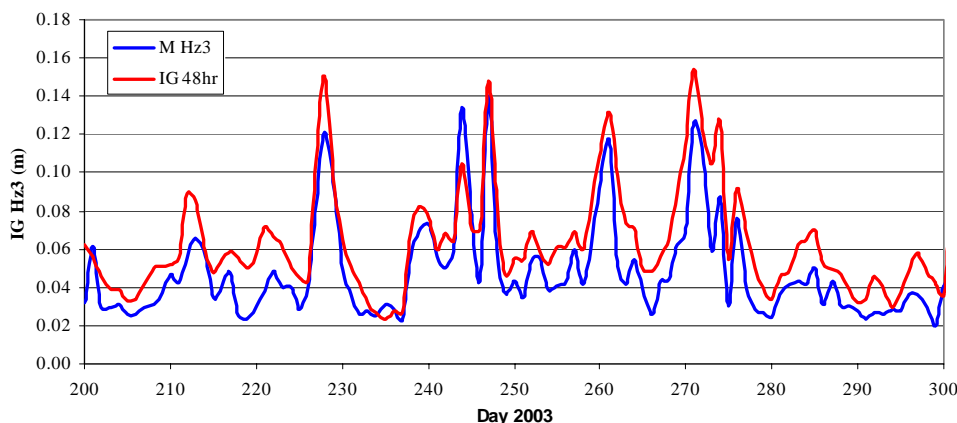


Figure 7. Time-series of the measured and 48-hour forecast IG wave heights inside the harbour basin (site M).

DISCUSSION

The measured IG waves in the harbour basin are likely to be influenced by resonance, particularly as the basin dimensions suggest a degree of seiche at 50-70 s is likely (e.g. Eqn. 3), which is within the frequency range of incident IG energy. Indeed, this may explain some of the scatter in the tidal modulation part, and modeling the long wave response of the harbour is being conducted to investigate this. Also, the IG forecast system relies on the accuracy of forecast swell height and period, and so a high resolution SWAN wave generation / transformation model has been subsequently nested within the larger deepwater model to improve the forecast accuracy.

Overall, the system provides a very clear and reliable indication of the timing and magnitude of the upcoming IG events. We note that Lara *et al* (2004) found a very similar relationship for IG waves near the entrance to Gijon harbour, which was consistent with several other coastal locations reported in the literature. This suggests the infragravity forecasting method could be applied to many harbour basins in the world, subject to onsite calibration.

CONCLUSIONS

An empirical formula to predict the infragravity waves at the Port Taranaki berths has been developed, based on the offshore (deepwater) partial significant swell height, associated peak period, and the tidal water level. A regional WAM model was used to forecast the swell height and period, and in turn predict the infragravity wave heights at the harbour berths. The system was found to reproduce all the major IG events up to 96 hours ahead, and predicted ~80% of the IG variance at 48 hours forecast. Implementation of the system as an operational tool for Port Taranaki harbour management has subsequently used a SWAN model for the regional wave generation and transformation (see www.metocean.co.nz).

ACKNOWLEDGEMENTS

Thanks to Westgate Port Taranaki and Capt. Ray Barlow for project support and to Brett Beamsley and David Johnson for constructive reviews and discussions.

REFERENCES

- Bowers, E.C.: 1982, The modelling of waves and their effects in harbours, in *Hydraulic Modelling in Maritime Engineering.*, Thomas Telford, London, 121-127.
- Funke, E. R. and Mansard E. P. D., 1979. On the synthesis of natural wave trains in deep water, *Proc. 17th Int. Conf. On Coast. Eng.*, Sydney, pp. 2974-2991.
- Goda, Y., 1983. Analysis of Wave Grouping and spectra of Long-travelled Swell, Report of the Portt and Harbour Research Institute, Vol 22, N° 1.
- Goring, D. G. 2005. A rissaga nowcasting system. *Proc. Waves 2005*, Madrid, 3-5 July, 2005.
- Gorman, R., 2005. Numerical wave modelling for the New Zealand region. *Proc. 2005 Pacific Coasts and Ports Conf.*, Adelaide, Australia.
- Kimura, A., 1980. Statistical properties of random wave groups, *Proc 17th Int. Conf. Coast. Eng.*, Sydney, pp. 2955-2973.
- Lara, J., Martin, F., Losada, I., and Diaz, G. 2004. Experimental analyses of long waves at harbour entrances. *Proc. 29th Int. Conf. Coastal Eng.*, Lisbon, Portugal, 19-24 September 2004.
- Longuet-Higgins, M., and R. Stewart, 1962. Radiation stress and mass transport in gravity waves, with application to "surf beat." *J. Fluid Mech.* vol. 13, pp. 481-504.
- McComb, P., Black, K., Healy, T. and Atkinson, P 1999. Coastal and sediment dynamics at Port Taranaki, New Zealand: a large, multi-faceted, field experiment. *Proc. Coastal Structures '99 Conf.*, Santander, Spain, pp. 823-832.
- Medina, J. R. 1990. The Dependency of Inshore Long waves on the Characteristics of Offshore Short Waves (Discussion), *Coastal Eng.*, 14,185-190.
- Mei, C.C., and Agnon, Y., 1989: Long-period oscillations in a harbour induced by incident short waves, *J. Fluid Mech.*, 208, 595-608
- Munk, W.H.: 1949, Surf beats, *Eos, Trans. Amer. Geophys. Un.*, 30, (6), 849-854.
- Nelson, R. C., P. D. Treloar y N. V. Lawson, 1988. The Dependency of Inshore Long Waves on the Characteristics of Offshore Short Waves. *Coastal Eng.* 12, pp 213-231.
- Okiihiro, M., and R. T. Guza, 1995. Infragravity energy modulation by tides. *J. Geophys. Res.* vol. 100, no. C8, pp. 16,143-16,148.
- Rabinovich, A.B., 1993, Long Ocean Gravity Waves: Trapping, Resonance, and Leaking (in Russian), *Gidrometeoizdat*, St. Petersburg, 325 p.
- Sawaragi, T., and Kubo, M.: 1982, Long-period motions of a moored ship induced by harbor oscillations, *Coast. Eng. Japan*, 25, 261-275.
- Tucker, 1950. Surf beats: Sea waves of 1 to 5 minute period. *Proc. R. Soc. London A*, 202, 565-573.
- Wiegel, R.L.: 1964, Tsunamis, storm surges, and harbor oscillations. Ch. 5 in *Oceanographical Engineering*, Prentice-Hall, Englewood Cliffs, N.J., 95-127.
- Wilson, B.: 1972, Seiches, *Advances in Hydrosiences*, 8, 1-94.
- Wu, J. K., and P. L. F. Lui, 1990. Harbour excitations by incident wave groups. *J. Fluid Mech.*, vol. 217, pp. 595-613.